The Retrieval of Planetary Boundary Layer Structure Using Ground-Based Infrared Spectral Radiance Measurements

WILLIAM L. SMITH

Atmospheric Sciences Division, NASA/Langley Research Center, Hampton, Virginia

WAYNE F. FELTZ, ROBERT O. KNUTESON, HENRY E. REVERCOMB, AND HAROLD M. WOOLF

Cooperative Institute for Meteorological Satellite Studies, University of Wisconsin—Madison, Madison, Wisconsin

H. BEN HOWELL

National Environmental Satellite and Data Information Service, NOAA, University of Wisconsin—Madison, Madison, Wisconsin

(Manuscript received 15 July 1997, in final form 18 March 1998)

ABSTRACT

The surface-based Atmospheric Emitted Radiance Interferometer (AERI) is an important measurement component of the Department of Energy Atmospheric Radiation Measurement Program. The method used to retrieve temperature and moisture profiles of the plantetary boundary layer from the AERI's downwelling spectral radiance observations is described.

1. Introduction

Use of ground-based instrumentation to obtain atmospheric temperature retrievals from infrared (IR) radiances was first suggested by Smith (1970). The advantage of using an interferometer system to sense lower tropospheric temperature and water vapor was first demonstrated at the Ground-based Atmospheric Profiling Experiment (GAPEX) in 1988 using the High-resolution Interferometer Sounder (HIS) aircraft instrument looking upward from the surface. Encouraging temperature and moisture retrieval results were obtained from the radiance data collected, which compared favorably to radiosonde data used as ground truth (Smith et al. 1990). Improvements in the system funded by the Department of Energy's (DOE) Atmospheric Radiation Measurement (ARM) program produced an Atmospheric Emitted Radiance Interferometer (AERI) prototype system and finally the current operational version of the instrument (Revercomb et al. 1993; Smith et al. 1993). AERI has evolved into a fully automated, self-calibrated (Revercomb et al. 1988) instrument that allows continuous monitoring of the atmospheric downwelling IR emission. This remote sensing approach is now being adopted elsewhere around the world (Spankuch et al. 1995).

The AERI radiances can be used to produce vertical temperature and water vapor profiles every 10 min (Feltz 1994; Feltz et al. 1995; Feltz et al. 1996; Smith et al. 1995) in the planetary boundary layer (PBL)—the lowest 3 km of the earth's atmosphere. AERI measures IR radiation spectra (3–18 μm) with a spectral resolution better than 1 cm^{-1} (Fig. 1). These radiance spectra are transformed to vertical temperature and water vapor profiles by inverting the radiative transfer equation (RTE). The 10-min time sampling allows high vertical and temporal resolution boundary layer information to be obtained during frontal passages, when rapid destabilization occurs as a result of surface heating and dry line passages and during other dynamic meteorological situations. Good temperature and water vapor retrieval skill using AERI to sound the PBL has been shown during numerous field experiments.

This paper presents the methodology used to retrieve atmospheric profiles of temperature and water vapor from AERI data. Statistical comparisons with radiosondes for both clear and cloudy conditions over a six-month period of operation at the DOE Cloud and Radiation Testbed (CART) site near Lamont, Oklahoma, are provided to illustrate the accuracy of the AERI sounding system. Example comparisons of time cross sections of boundary layer structure observed by AERI and 3-hourly interval radiosondes are presented to dem-

Corresponding author address: William L. Smith, NASA/Langley Research Center, Atmospheric Sciences Division, MS-401, Hampton, VA 23681-0001.
E-mail: bill.1.smith@larc.nasa.gov

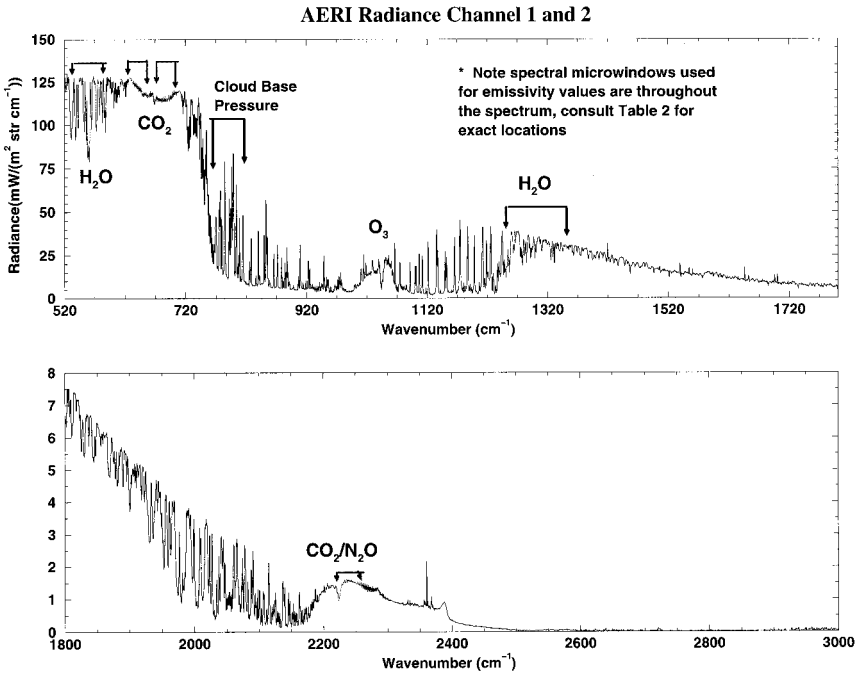

FIG. 1. A radiometric observation of both radiance bands vs wavenumber showing the spectral regions used in the AERI retrieval algorithm. Please consult Table 1 for specific quantitative wavenumber regions.

onstrate the ability of the AERI system to resolve significant thermodynamic features of the PBL with high time resolution.

2. Retrieval methodology

The AERI retrieval is accomplished in two steps. 1) An initial temperature and water vapor profile is obtained using nearby radiosonde observation, forecast profile, or an estimate based on a statistical regression formed from a climatological set of radiosonde data, and 2) an iterative recursive physical solution of the radiative transfer equation, using the results of 1) as the initial profile, is conducted to yield a final measure of the temperature and water vapor profile.

The profile retrieval process requires the use of an initial, or guess, temperature and water vapor profile (Smith 1970). This initial profile serves as a first guess to constrain the result to a reasonable solution, which is particularly important in atmospheric regions where the profile information content of the radiances is weak (i.e., above the PBL for this case). The initial profile is obtained here using a 2-yr radiosonde climatology for the Southern Great Plains (SGP) DOE CART site. This dataset is used to develop regression equations that are used to provide an initial profile for each retrieval based on the actual radiance observations associated with that retrieval. The development of the ''regression guess'' relations is described as follows.

TABLE 1. Spectral regions used for calculating temperature and water vapor mixing ratio in the AERI retrieval algorithm.

Temperature	Water vapor
612–618 cm^{-1}	538–588 cm^{-1}
624–660 cm^{-1}	1250–1350 cm^{-1}
674–713 cm^{-1}	
2223–2260 cm^{-1}	

A fast forward model calculation (described later) of spectral radiance, as would be observed by AERI, is performed for each radiosonde case to provide a radiosonde–spectral radiance pair for the statistical regression analysis. A regression analysis is then applied to relate these theoretical calculations of radiance, for the spectral regions listed in Table 1 and illustrated in Fig. 1, and the matching radiosonde temperature and water vapor profiles. The resulting regression equations allow the specification of an excellent initial profile of atmospheric state, as needed for a physical solution of the RTE, from every AERI observation. Total precipitable water (TPW) and/or surface humidity can also be used as a predictor in the regression. This allows the use of microwave radiometer (Han et al. 1994) or global positioning system (GPS)-derived TPW (Businger et al. 1996; Ware et al. 1996) and/or surface observations to be used as additional information to better constrain the statistical retrieval used as the initial profile in the physical retrieval process.

A schematic of the retrieval technique can be seen in Fig. 2. In practice, microwave radiometer TPW may not

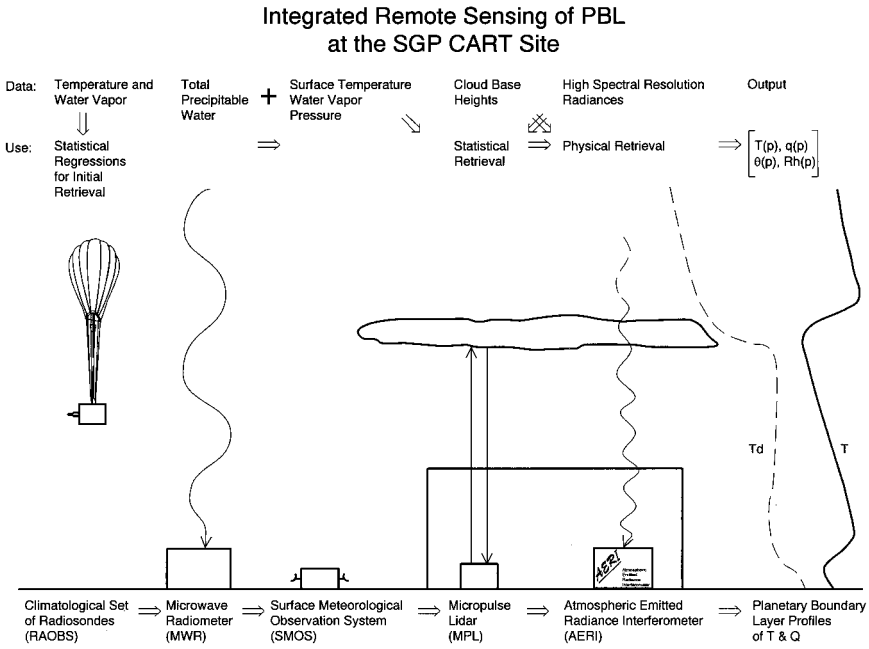

FIG. 2. A schematic of the AERI retrieval process at the SGP CART site. Microwave radiometer total precipitable water and surface water vapor data are only used to improve the first guess and are not necessary to do retrievals. The AERI physical retrieval algorithm will change the first guess to fit the observed radiances without any auxiliary data.

be available for use in the AERI retrieval. To cope with this possibility, separate sets of regression equations are derived that exclude these data as predictors for use when these data are missing. Comparisons of retrievals conducted with and without the use of TPW observations indicate that the degradation of the resulting retrieval produced by the loss of these data is limited to the layer between 1500 and 3000 m. The additional information TPW offers impacts only where AERI water vapor weighting functions are rapidly decaying. Surface mixing ratio is easily measured with a sensor on the AERI system or a nearby meteorological surface station.

A physical iterative and recursive solution of the RTE provides the final temperature and moisture profile retrieval. The final solution, obtained through iterative application of an inverse of a simplified RTE, satisfies the observed AERI spectrum through minimal adjustment of the initial regression guess profiles. During each iteration, temperature and water vapor mixing ratio adjustments are made to minimize the differences between observed and calculated spectra. The physical retrieval algorithm usually converges within 10 iterations.

The radiative transfer equation to be inverted is

$$R_\nu = -\int_{p_s}^{0} B_\nu(T)\frac{d\tau_\nu(p_s, p)}{dp}\,dp, \qquad (1)$$

where $\tau_\nu(p_s, p) = \exp[1/g \int_{p_s}^{p} (k + k'_q)q\,dp]$, R_ν is the spectral radiance at wavenumber ν, $\tau_\nu(p_s, p) = \Pi_i\,\tau_i(p_s, p)$ is the total transmittance of the atmosphere between the surface and pressure (p_s is pressure p at surface s), Π_i is the product of i absorbers, $B_\nu(T)$ is the Planck radiance corresponding to temperature T, p is the atmospheric pressure, g is acceleration due to gravity, k and k' are the absorption line and continuum absorption coefficients, respectively, and q_i is the mixing ratio of the ith absorbing gas. In case of clouds, the cloud component of transmittance is given by

$$\tau_{\text{cld}}(p_s, p) = 1.0 \qquad \text{for } p_c < p \le p_s,$$

and

$$\tau_{\text{cld}}(p_s, p) = (1 - \epsilon_c) \quad \text{for } p \le p_c, \qquad (2)$$

where p_c is the cloud-base pressure and ϵ_c is the effective cloud emissivity. Equations (1) and (2) neglect the reflection of ground radiation from clouds. Since most of the channels used to retrieve temperature and water vapor are within high absorption regions, this additional source of energy is negligible. However, in window regions this contribution may be important. The procedure used to define these cloud parameters from the AERI spectra can be found in Smith et al. (1993) and is outlined below.

Equation (1) is solved for the water vapor mixing ratio $q(p)$ and atmospheric temperature $T(p)$ through a mathematical linearization of the RTE and an inverse solution obtained using a numerical recursion process. Linearization leads to the perturbation form (see the appendix)

$$\delta R_\nu = -\int_{p_s}^{0} \delta T W_\nu(T)\,dp - \int_{p_s}^{0} \delta q_i W_\nu(q_i)\,dp, \qquad (3)$$

where δ is a perturbation from the guess or prior solution; T is temperature; W is the weighting function for temperature, $W_\nu(T)$, and water vapor, $W_\nu(q)$; and q_i is the mixing ratio of the unknown absorbing gas profile (i.e., water vapor mixing ratio). The frequency dependence of R and W is understood. Specifically (from the appendix),

$$W_\nu(T) = -\left(\frac{\delta B_\nu}{\delta T}\right)^0 \frac{d\tau(p_s, p)}{dp}$$

and

$$W_\nu(q_i) = k_0\left[B_\nu(T^o)\tau(p_s, p) + \int_p^0 B_\nu(T)\frac{d\tau(p_s, p)}{dp}\,dp\right],$$

where the zero superscript refers to the guess condition and

$$k_0 = \frac{1}{g}(k + 2k'\overline{q_i}) = -\frac{d\delta\,\ln\tau_i(p_s, p)}{\delta q_i dp},$$

and the frequency dependence of all quantities, except T and q, is understood.

The weighting functions decrease exponentially with increasing altitude, with the rate dependent on the strength of the absorption. Thus, the radiance signals δR_ν are dominated by contributions from near the surface with rapidly decreasing sensitivity to contributions from aloft. This altitude sensitivity characteristic leads to numerical instability of the direct inverse of (3) because of the strong correlation of the weighting functions among different spectral channels (i.e., lack of linear independence of the system of equations). However, the rapidly diminishing sensitivity of the observed radiance with altitude enables a very stable recursive procedure to be used, whereby the temperature and moisture mixing ratio values are obtained in a subsequential fashion starting at the surface and moving upward in altitude. Assuming for each recursive step that δT and δq are independent of pressure for $p \le p'$, a system of two equations with two unknowns for each level is obtained:

$$R^*_{T_{p'}} = \delta T_{p'} T^*_{T_{p'}} + \delta q_{p'} Q^*_{T_{p'}}$$

and

$$R^*_{q_{p'}} = \delta T_{p'} T^*_{q_{p'}} + \delta q_{p'} Q^*_{q_{p'}}, \tag{4}$$

where

$$R^*_{p'}(T) = \sum_\nu W_\nu(T_{p'}) \times \left\{\delta R_\nu - \int_{p'}^{p_s} [\delta T W_\nu(T) + \delta q W_\nu(q)]\,dp\right\},$$

$$R^*_{p'}(q) = \sum_\nu W_\nu(q_{p'}) \times \left\{\delta R_\nu - \int_{p'}^{p_s} [\delta T W_\nu(T) + \delta q W_\nu(q)]\,dp\right\},$$

$$T^*_{T_{p'}} = \sum_\nu W_\nu(T_{p'}) \int_0^{p'} W_\nu(T)\,dp,$$

$$Q^*_{T_{p'}} = \sum_\nu W_\nu(T_{p'}) \int_0^{p'} W_\nu(q)\,dp,$$

$$T^*_{q_{p'}} = \sum_\nu W_\nu(q_{p'}) \int_0^{p'} W_\nu(T)\,dp, \quad \text{and}$$

$$Q^*_{q_{p'}} = \sum_\nu W_\nu(q_{p'}) \int_0^{p'} W_\nu(q)\,dp.$$

Note that the quantity in { } is the residual radiance not accounted for by the solution at the levels below p' (i.e., $p > p'$). Thus, the recursive process starts with $p' = p_s$, in which case the integral quantity in the { } is zero. The recursive process is iterated until the residuals $R^*_{p'}(T)$ and $R^*_{p'}(q)$ become smaller than the noise level of the measurements in a spectral rms sense.

In the solution for the temperature and water vapor profiles, the spectral regions used (Table 1) are pure from the point of view of not being affected by a nonuniformly mixed gas other than water vapor (i.e., spectral regions where ozone, carbon monoxide, methane, chlorofluorocarbons, etc., are significant are avoided for the temperature and water vapor retrieval). Also, to minimize the impact of clouds on the retrieval, spectral regions that are relatively transparent to IR radiation (i.e., ''windows'') are used to define cloud parameters (altitude and emissivity) and are not included in the system of equations used in the profile retrieval process.

The pressure of the cloud base is specified using the initial temperature profile and a cloud-base height supplied by simultaneous ceilometer or micropulse lidar measurements. In the absence of these direct measurements of cloud-base altitude, it is specified from semitransparent carbon dioxide absorption channel radiances and neighboring window channel radiances. Since carbon dioxide is a uniformly mixed gas, the carbon dioxide depth from the surface to the cloud is directly proportional to the difference between the cloud pressure and the surface pressure. Specifically, it can be shown that

$$\frac{R_1 - R_1^o}{R_0 - R_0^o} = \frac{\displaystyle\int_{p_c}^0 B_1(T)\,d\tau_1(p_s, p) + B_1(T_c)\tau_1(p_s, p_c)}{\displaystyle\int_{p_c}^0 B_0\,d\tau_0(p_s, p) + B_0(T_c)\tau_0(p_s, p_c)}, \tag{5}$$

where it is assumed that the cloud emissivity for the carbon dioxide absorption line and the neighboring window (i.e., in between neighboring carbon dioxide lines) is constant; p_c is the cloud pressure; R_1, R_0 are the observed radiances; R_1^o, R_0^o are the calculated clear column radiances; and subscripts 0, 1 are the window and carbon dioxide absorption channel frequencies, respectively.

TABLE 2. Spectral wavenumbers (cm^{-1}) used for calculating cloud-base pressure and cloud emissivity.

Cloud-base pressure	Emissivity					
750–800 cm^{-1}	558.8	826.2	1069.8	1216.7	1899.82	2083.7
	588.2	832.1	1095.0	1222.47	1929.97	2088.3
	607.0	837.3	1103.76	1227.93	1952.3	2092.2
	746.0	845.7	1109.16	1231.45	1958.71	2096.2
	747.6	850.9	1114.9	1234.44	1973.8	2101.9
	749.25	856.6	1119.09	1238.18	1979.1	2104.4
	757.95	862.4	1128.5	1241.39	1982.8	2109.5
	759.6	868.5	1144.7	1247.0	2004.2	2112.5
	761.3	875.2	1150.4	1250.4	2011.6	2118.0
	762.75	880.0	1159.69	1255.75	2024.8	2126.0
	764.22	885.2	1168.23	1262.7	2031.2	2133.12
	765.65	893.8	1177.8	1264.4	2035.7	2143.2
	768.06	901.9	1179.7	1274.3	2038.8	2149.7
	773.3	916.5	1182.5	1275.98	2045.3	2159.2
	781.3	963.2	1189.7	1278.4	2049.6	2164.4
	789.3	992.1	1192.3	1282.2	2055.85	2168.28
	800.8	1013.0	1194.4	1285.3	2057.27	2173.5
	805.15	1021.7	1200.5	1291.7	2062.12	2177.3
	807.04	1036.0	1204.1	1293.8	2070.5	2188.6
	811.65	1043.85	1207.7	1298.8	2075.7	2190.9
	821.0	1064.2	1214.1	1300.7	2080.55	2223.0

Note that for high clouds where $d\tau(p_s, p) \cong 0$ for $p \leq p_c$,

$$f(p_c) = \frac{R_1 - R_1^o}{R_0 - R_0^o} \approx \tau_1(p_s, p_c), \tag{6}$$

assuming $\tau_0(p_s, p_c) \cong 1$. Thus, the cloud pressure function $f(p_c)$ is mainly dependent on the transmittance of the atmosphere between cloud and ground, which for carbon dioxide is proportional to the pressure difference between cloud and ground. In numerical practice, p_c is specified as that value that minimizes the difference between the left- and right-hand sides of Eq. (5) over a relatively large set of spectral channels (750–800 cm^{-1}) used for this process. Cloud pressure is estimated prior to the determination of T and q in each iterative step using prior solutions of T and q for computations of the R, $B(T)$, and $\tau(p_s, p)$ terms in (5).

The effective cloud emissivity spectrum needed for (2) is estimated by linear interpolation between window wavelengths (see Table 2) across the spectrum. The emissivity for the window wavelengths is determined using the relation

$$\epsilon_c = \frac{R_\nu - R_\nu^o}{R_\nu^B - R_\nu^o}, \tag{7}$$

where R^B equals the opaque cloud radiance [i.e., $B(T_c)\tau(p_s, p_c) - \int_{p_s}^{p_c} B(T)\, d\tau(p_s, p)$] computed from previous solutions for T and q and the cloud-base pressure specified from lidar data or using (5) above.

Thus, retrievals can be achieved beneath clouds. The three requirements to obtain an accurate temperature and water vapor retrieval from the surface up to the cloud-base altitude are

1) a good initial profile (i.e., the statistical regression retrieval),
2) a good definition of cloud-base altitude (obtained by a simultaneous ceilometer measurement, a concurrent micropulse lidar measurement, or by the CO_2/window channel radiative transfer procedure outlined above), and
3) cloud emissivity [calculated using (7) within the retrieval algorithm].

A necessary component for performing AERI retrievals in real time (within a 10-min window) is a fast forward model obtained by regressing optical depth from a line-by-line transmittance model against parameters obtained from the temperature and water vapor mixing ratio profiles. Effective absorption coefficients for radiatively active constituents (i.e., H_2O, O_3, CH_4, etc.) are calculated using FASCODE (Clough et al. 1981) and the HITRAN database (Rothman et al. 1992) for a diverse set of radiosonde measurements. A rapid regression transmittance model (fast model) is then derived using these effective absorption coefficients (Eyre 1991). The fast transmittance model provides the basis for rapid calculation of radiances needed to solve the system of equations above.

To correctly account for forward model spectroscopy and regression errors, determining a bias error spectrum for the retrieval algorithm is necessary. That is, when converging to a solution using the recursive method above, a bias must be added to the calculated radiance to alleviate systematic computation errors and instrumental bias errors. Historically, differences between calculated and observed radiances are obtained from clear radiosonde profiles of temperature and water vapor and

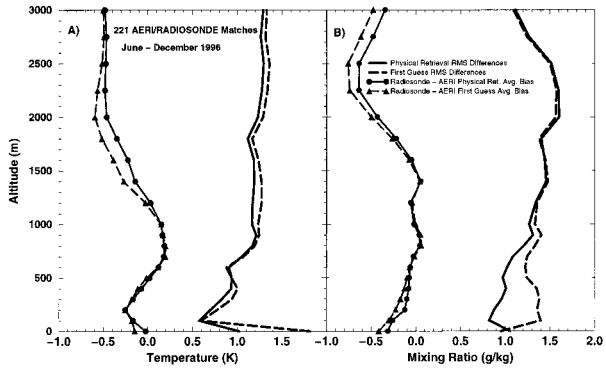

FIG. 3. AERI retrieval statistics for cases from June 1996 to December 1996 compared to a radiosonde (221 matches). (a) AERI retrieval temperature rms differences from radiosonde for both the regression first guess (long dashed) and final physical retrieval (solid black). Also displayed are mean differences for the same matches for first guess (dashed triangles) and physical retrievals (solid circles). (b) The same comparison except for water vapor mixing ratio.

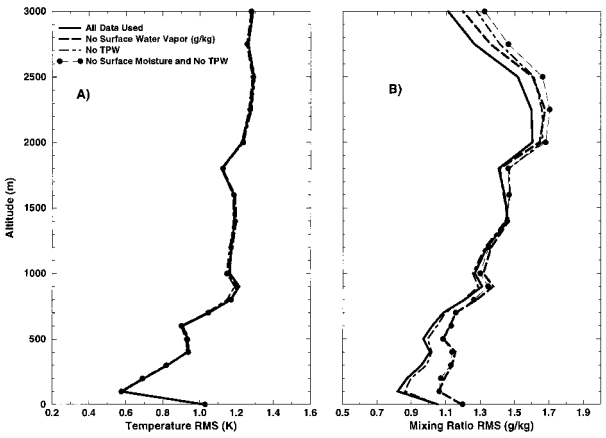

FIG. 4. AERI retrievals compared to radiosonde rms statistics for (a) temperature and (b) mixing ratio, indicating sensitivities to providing auxiliary surface moisture information and microwave radiometer TPW. The statistics were calculated using the same 221 matches shown in Fig. 3. The best agreement between AERI physical retrievals and radiosonde moisture measurements occur when both a surface moisture measurement and microwave TPW are used [solid black line in (b)]. A good measure of surface moisture improves the lower 1500 m of the physical retrievals [dot–dashed line in (b)], while microwave radiometer TPW slightly improves the profiles from 1500 to 3000 m [long dashed line in (b)]. The additional moisture information provided to the first guess has little impact on the temperature profile rms differences (a).

coincident AERI observations. Several of these residual differences are averaged to obtain a bias spectrum. The bias used in the AERI retrieval statistics shown below was based on calculated spectra for 20 carefully selected radiosondes and corresponding AERI spectral radiance observations during September 1996. This same bias, used for all times throughout the year, has proven to provide satisfactory results.

3. Results

AERI spectra are processed in a real-time mode, providing temperature and moisture retrievals for a large variety of climatological and atmospheric conditions in the clear sky or below cloud base. The accuracy of temperature retrievals is demonstrated to be better than 0.6 to 1.3 K from the surface to 3 km (see Fig. 3a, solid line), and mixing ratio retrieval differences (see Fig. 3b, solid line) are between 0.8 to 1.4 g kg^{-1}, as judged using coincident radiosondes over a six-month period (221 cases) at the SGP ARM site near Lamont. The dashed lines show AERI retrieval first-guess differences from radiosondes before the physical retrieval algorithm reduces the spectral residuals. Improvement in temperature is noted at all altitudes, while most of the water vapor information is added in the first 1500 m of the atmospheric column. A mean bias is presented in Fig. 3 (solid line with dots), indicating average differences between radiosonde and AERI retrievals to be near zero until 1500 m for both temperature and water vapor. AERI retrievals on average are moister and warmer than radiosonde measurements from 1500 to 3000 m. The regression first-guess bias appear to have the same features as indicated (dashed line with triangles) in Fig. 3. The AERI physical retrieval algorithm reduces the first-guess mean bias for both temperature and water vapor toward zero at all levels. While the physical retrieval tries to correct the first guess to fit the observed radiances, a mean difference of as great as 0.5 K and 0.7 g kg^{-1} relative to radiosondes still exists above 1500 m. It is believed that further work on the fast forward model will reduce this bias aloft.

Figure 4 shows the physical retrieval sensitivity to the microwave radiometer TPW and surface moisture information to the first guess (Fig. 2). These additional data have negligible impact (Fig. 4a) on temperature. For moisture (Fig. 4b), a reduction in rms differences with radiosondes occurs in the lowest 1500 m when a well-calibrated surface moisture value is inserted at the surface point in the first guess used for the physical retrieval (dot–dashed line). The rms differences are reduced by as much as 0.3 g kg^{-1}. Using TPW as a predictor in the first guess improves rms differences from 1500 to 3000 m by 0.1 g kg^{-1}. However, final physical AERI retrievals have nearly the same rms differences in the lowest 1500 m, indicating that AERI physical retrievals are insensitive to additional TPW predictor information within the first guess in the lower part of the PBL. The best agreement between radiosonde and AERI physical retrieval moisture profiles occur when both a surface mixing ratio and a microwave TPW measurement are used (black solid line).

The rms differences for the physical retrievals (solid lines) shown in Fig. 3 should be considered as an upper bound for AERI retrieval error since the radiosondes possess measurement errors particularly for water vapor, and the columns of atmosphere sampled differ because of the horizontal motion of the ascending balloon. In

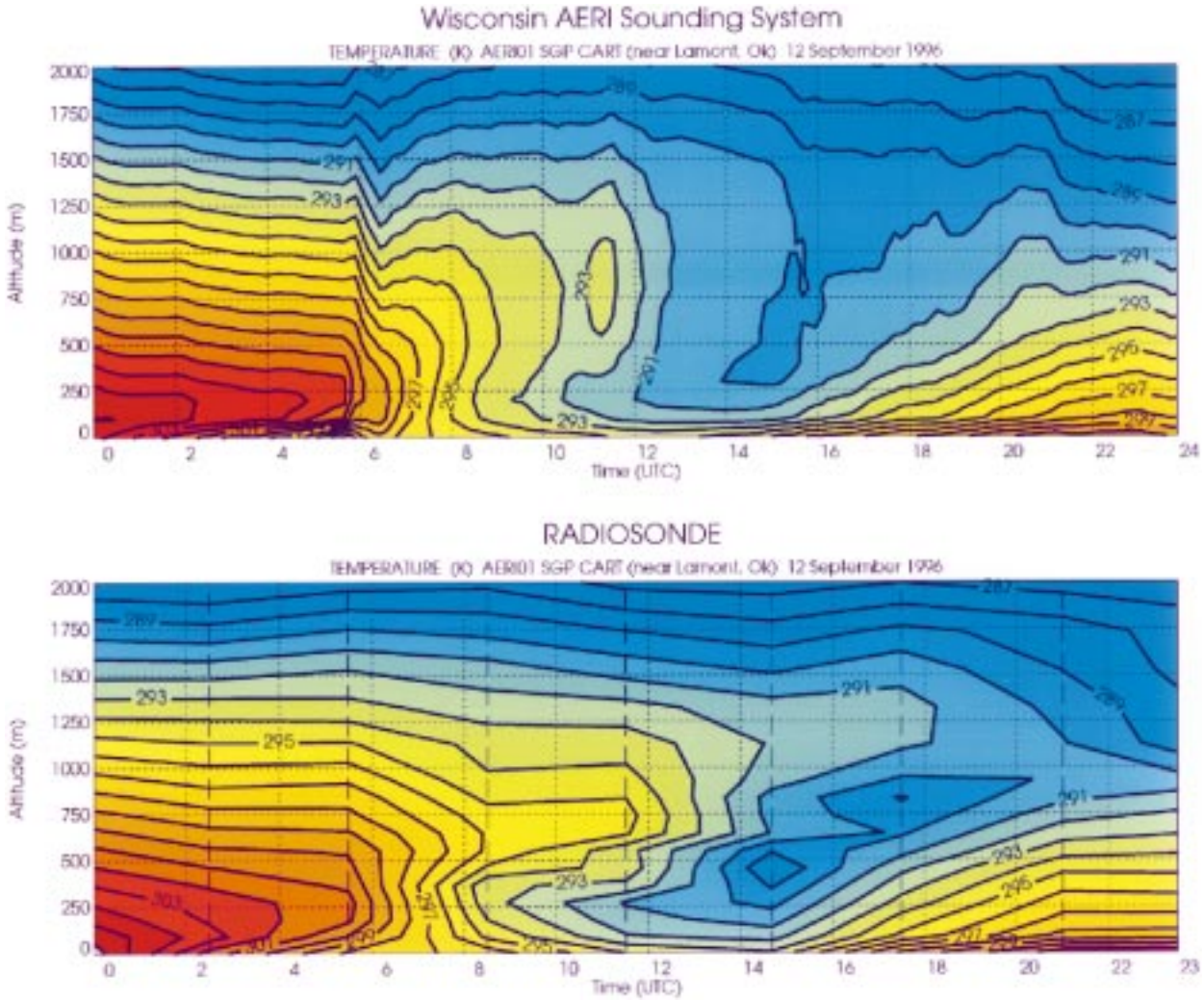

FIG. 5. Example of AERI boundary layer temperature retrievals compared to an interpolated radiosonde cross section (radiosonde locations are indicated by the heavy dashed lines), indicating a cold frontal passage at 0600 UTC.

general, radiosonde errors are on the order of 0.5°C and 10% for temperature and relative humidity, respectively (Pratt 1985; Schmidlin 1988), indicating that the actual errors in the AERI retrievals are significantly smaller than the estimates shown in Fig. 3.

With good retrieval accuracy and high temporal resolution, the AERI instrument can be utilized to study mesoscale meteorological features that may not be resolved by direct measurement as a result of infrequent radiosonde launches. Figure 5 demonstrates AERI's capabilities for resolving spatial features that 3-hourly radiosonde launches observe but with higher temporal frequency. On 12 September 1996, a cold front passed through the Lamont area. AERI resolved the rapid vertical temperature decrease at approximately 0600 UTC. An interpolation between radiosondes launched 3 h apart indicates the same feature. Since the normal frequency of radiosonde launches is 12 h, the AERI will provide better resolution of the PBL features than operational radiosonde measurements. It is also worthy to note that the vertical resolution of the AERI retrievals is somewhat inferior to the point measuring radiosondes. However, the high time frequency of the AERI sounding provides some compensation in terms of providing significant thermodynamic temporal structure information of the PBL. Note that the radiosonde information exists at the long dashed lines. Figure 6 shows the same frontal passage, but instead AERI water vapor mixing ratio profiles are compared to Raman lidar (Melfi et al. 1985; Goldsmith et al. 1994) and radiosondes. Notice that the AERI and Raman lidar indicate rapid absolute moistening of the PBL at 0600 UTC, while the radiosondes appear to miss the airmass transition due to launches on either side of the frontal passage. AERI retrievals also resolve the elevated water vapor layer at 1 km, also present in the Raman and radiosonde cross sections. Active Raman lidar profiles also have higher vertical resolution than AERI due to the active system's capa-

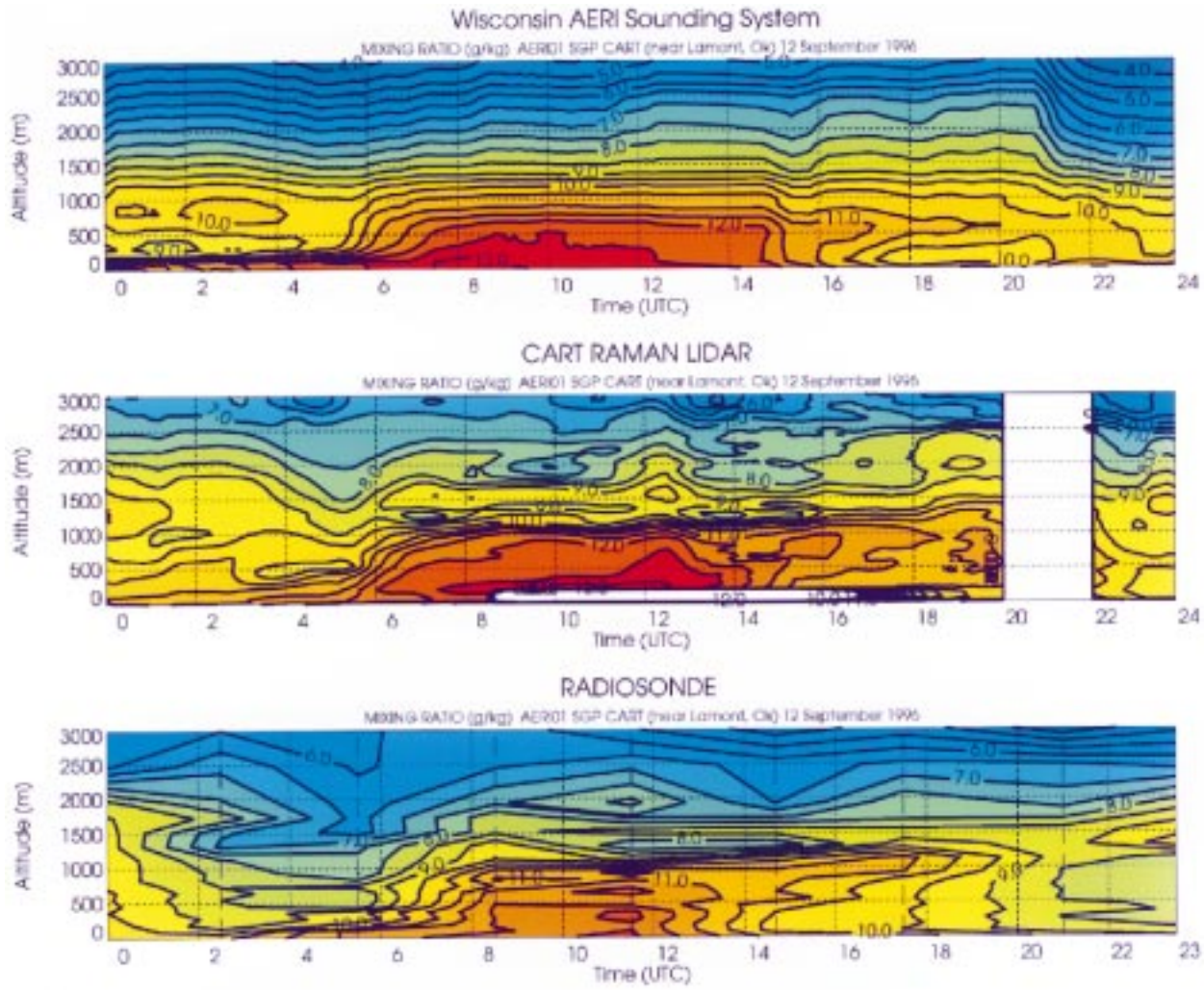

FIG. 6. Example of AERI boundary layer water vapor retrievals compared to Raman lidar and interpolated radiosonde cross sections (radiosonde locations as in Fig. 5), indicating AERI and lidar agreement in water vapor increase and an elevated layer of moisture occurs between 1600 and 2200 UTC.

bility to range gate (i.e., altitude layer restrict) the energy sensed. Raman lidar has proven to be a very valuable research tool for verifying AERI retrieval accuracy, but due to high production cost, it is not yet practical for widespread operational implementation.

It is important to note that Figs. 5 and 6 were constructed from AERI retrievals for both clear and cloudy conditions. The cloud-base altitudes ranged from 5 to 12 km during the day shown with the lowest clouds being observed near the time of frontal passage.

4. Vertical resolution of retrieved profiles

The vertical resolution of the retrieved profiles is estimated by analyzing the vertical interlevel covariance of the errors in the retrieved temperature and water vapor values. The error in the retrieval is approximated as the difference between the retrieved values and radiosonde observations. Assuming that there is no bias component to the errors of the radiosonde observations (i.e., no vertical correlation of the radiosonde errors of measurement), then the vertical covariance of the retrieval error represents the vertical resolution of the retrieved temperature and water vapor values.

Mathematically, the covariance between the error of retrieved temperature at one level with the error in temperature at all other levels is given by

$$\mathbf{C}(Z_o, Z) \equiv \frac{\sum_{i=1}^{N} [T_r(Z_o) - T(Z_o)][T_r(Z) - T(Z)]}{\sqrt{\sum_{i=1}^{N} [T_r(Z_o) - T(Z_o)]^2 \sum_{i=1}^{N} [T_r(Z) - T(Z)]^2}},$$

where N is the number of retrieval and radiosonde pro-

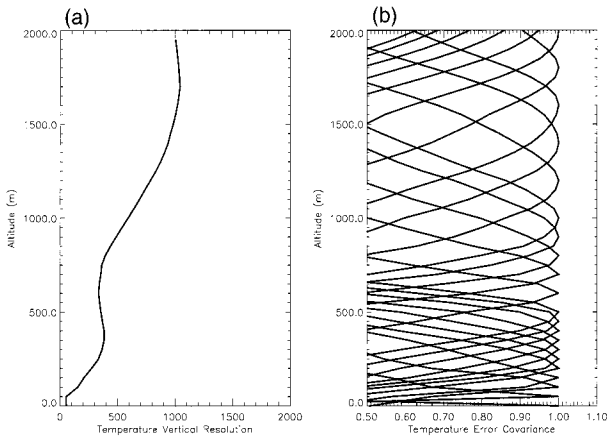

FIG. 7. (a) Vertical temperature resolution and (b) vertical temperature covariance functions as estimated through radiosonde intercomparisons with AERI retrievals.

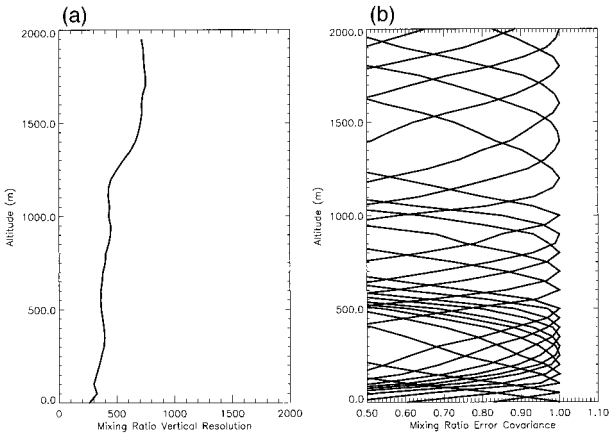

FIG. 8. Same as Fig. 7 but for atmospheric water vapor mixing ratio.

file comparisons, T_r is the retrieved temperature, T is the true temperature approximated from a radiosonde observation, Z is the altitude, and Z_o is the altitude for which vertical resolution function is being defined. As $T_r(Z_o)$ approaches $T(Z_o)$, for all Z_o, the matrix $\mathbf{C}$ (Z_o, Z) approaches the identity matrix.

Figures 7 and 8 show the AERI retrieval error vertical covariance functions for temperature and water vapor, respectively. Figures 7a and 8a show the vertical resolution of the retrieved temperature and moisture profiles as defined from the half-width of the covariance functions for each atmospheric level (i.e., the vertical distance between the 0.5 covariance values). As shown, the vertical resolution for temperature is nearly infinite at the surface decreasing rapidly to about 400 m within the lowest 1 km and to about 1000 m at the 2-km level. The water vapor vertical resolution within the lowest 1 km is almost constant at 400 m. The resolution degrades to about 800 m at 2 km above the surface.

Note that the vertical resolution for water vapor degrades more slowly with altitude than does the vertical resolution for temperature. This characteristic is believed to be due to the fact that water vapor mixing ratio decreases in a near-exponential fashion. The temperature profile is derived from CO_2 emission, and the CO_2 mixing ratio is uniform with respect to altitude. As a consequence, water vapor emission for different wavelengths emanates from narrower layers of the atmosphere than does CO_2 emission for different wavelengths of measurement.

These resolution estimates are a lower limit due to the relatively coarse vertical quadrature used for the retrieval (see Table 3) and because of vertically correlated errors in the rapidly ascending radiosonde measurements. A similar analysis using active remote sensing measurements (i.e., Raman lidar for water vapor and a radio acoustic sounding system for temperature) will be performed to validate the estimates of AERI profile retrieval resolution shown here.

5. Future directions

AERI is used to monitor the change of the thermodynamic structure in the planetary boundary layer. Good skill has been shown for the SGP CART site over two years. Example meteorological applications of this PBL sounding technique are given by Feltz et al. (1998). Future research includes combining *GOES-8* sounding radiances with AERI sounding radiances to produce full tropospheric vertical profiles of temperature and water vapor. The retrieval algorithm, soon to be implemented, includes a new and improved fast transmittance model based on the Line-By-Line Radiative Transfer Model (Clough et al. 1989). More retrieval levels are also being added to the algorithm in the first 2 km, from the surface upward, to better optimize the vertical resolution available in the AERI radiances and to minimize quadrature error. Finally, the AERI PBL profiles will be used to study the improvement in mesoscale forecast models when retrievals are available from the grid of five AERIs in the Southern Great Plains of the United States.

TABLE 3. Nominal* pressure levels (mb) used for calculating temperature and mixing ratio profiles.

1000	950	900	800	700	600	350	150	30	7
990	940	880	780	680	550	300	125	25	5
980	930	860	760	660	500	250	100	20	4
970	920	840	740	640	450	200	75	15	3
960	910	820	720	620	400	175	50	10	2

* Actual pressure levels used are based on observed surface pressure where $p = p$(nominal)*[psfc/psfc(nominal)].

APPENDIX

Form of Radiative Transfer Equation Inverted for Atmospheric Temperature and Water Vapor Profile Using AERI Data

The radiative transfer equation governing the downwelling spectral radiance at the surface ($p = p_s$) is

$$R_\nu = -\int_{p_s}^{0} B_\nu(p)\frac{d\tau_\nu(p_s, p)}{dp}\,dp,$$

where ν is the spectral wavenumber, p is the atmospheric pressure, B is the Planck radiance, and τ is the atmospheric transmittance. Considering a deviation from a ''guess'' state denoted by a zero superscript (ν subscript omitted),

$$\delta R = R - R^o = -\int_{p_s}^{0} B\frac{d\tau}{dp}\,dp + \int_{p_s}^{0} B^o\frac{d\tau^o}{dp}\,dp$$

since $\delta B \equiv B - B^o$ and

$$\delta R = -\int_{p_s}^{0} \delta B\frac{d\tau}{dp}\,dp - \int_{p_s}^{0} B^o\frac{d(\delta\tau)}{dp}\,dp, \quad \text{(A1)}$$

where $\delta\tau \equiv \tau - \tau^o$.

To express δR in terms of the desired profile variables T and q, where T is the atmospheric temperature and q is the mixing ratio of the absorbing gas (e.g., water vapor), we use the linear approximation

$$\delta B = \left(\frac{\delta B}{\delta T}\right)^o \delta T, \quad \text{(A2)}$$

where

$$\left(\frac{\delta B}{\delta T}\right)^o = \left.\frac{\delta B}{\delta T}\right|_{T=T^o},$$

and the relation is

$$\delta\tau = \tau\delta\,\ln\tau.$$

Assuming that the total transmittance is given by the product of the uniformly mixed gases and the transmittance of atmospheric water vapor, and assuming $\delta\tau_d = 0$,

$$\delta\tau = \tau\delta\,\ln\tau_w$$

and

$$d(\delta\tau) = \tau d(\delta\,\ln\tau_w) + \delta\,\ln\tau_w d\tau, \quad \text{(A3)}$$

where τ is the total transmittance and τ_w is the water vapor transmittance since

$$\tau_w = \exp\left[\frac{1}{g}\int_{p_s}^{p}(k + k'q)q\,dp\right],$$

where g is the acceleration due to gravity. The terms k and k' are absorption line and continuum absorption coefficients:

$$\delta\,\ln\tau_w = \frac{1}{g}\int_{p_s}^{p}\{[(k + k'q)q - (k + k'q^o)q^o]\,dp\}$$

$$\delta\,\ln\tau_w = \frac{1}{g}\int_{p_s}^{p}[k(q - q^o) + k'(q + q^o)(q - q^o)]\,dp$$

$$\delta\,\ln\tau_w = \frac{1}{g}\int_{p_s}^{p}(k + 2k'\overline{q})\delta q\,dp = -\int_{p_s}^{p} k_o\delta q\,dp, \quad \text{(A4)}$$

where $\overline{q} = (q + q^o)/2$ and $k_o = (1/g)(k + 2k'\overline{q})$. Then substituting (A4) into (A3) into (A2) into (A1) yields

$$\delta R = \int_{p_s}^{0}\delta TW_T\,dp + \int_{p_s}^{0} k_oB^o\tau\delta q\,dp + \int_{p_s}^{0} B^o\left(\int_{p_s}^{p} k_o\delta q\,dp\right)\frac{d\tau}{dp}\,dp, \quad \text{(A5)}$$

where W_T is the temperature profile weighting function $-(\delta B/\delta T)^o\,(d\tau/dp)$. We now integrate the third term on the right of (A5) by parts, letting $u \equiv \int_{p_s}^{p} k_o\delta q\,dp$ and $v \equiv \int_{p_s}^{p} B^o(d\tau/dp)\,dp$. Since $\int u\,dv \equiv uv - \int v\,du$, then

$$\int_{p_s}^{0} B^o\left(\int_{p_s}^{p} k_o\delta q\,dp\right)\frac{d\tau}{dp}\,dp = \left(\int_{p_s}^{p} k_o\delta q\,dp\int_{p_s}^{p} B^o\frac{d\tau}{dp}\,dp\right)_{p_s}^{0} - \int_{p}^{0}\left(\int_{p_s}^{p} B^o\frac{d\tau}{dp}\,dp\right)k_o\delta q\,dp,$$

or

$$\int_{p_s}^{0} B^o\left(\int_{p_s}^{p} k_o\delta q\,dp\right)\frac{d\tau}{dp}\,dp = \int_{p_s}^{0} k_o\delta q\,dp\int_{p_s}^{0} B^o\frac{d\tau}{dp}\,dp - \int_{p_s}^{0}\left(\int_{p_s}^{p} B^o\frac{d\tau}{dp}\,dp\right)k_o\delta q\,dp,$$

$$\int_{p_s}^{0} B^o\left(\int_{p_s}^{p} k_o\delta q\,dp\right)\frac{d\tau}{dp}\,dp = \int_{p_s}^{0} k_o\delta q\int_{p}^{0} B^o\frac{dz}{dp}\,dp. \quad \text{(A6)}$$

Substituting (A6) into (A5) yields

$$\delta R = \int_{p_s}^{0}\delta TW_T\,dp + \int_{p_s}^{0}\delta qW_q\,dp, \quad \text{(A7)}$$

where

$$W_q = k_o\left[B^o\tau + \int_p^0 B^o\frac{d\tau}{dp}\,dp\right].$$

Note that the constant k_o can be defined from (A4),

$$k_o = \frac{-d\delta\,\ln\tau_w}{\delta q\,dp} \approx \frac{-d\,\ln[\tau_w(q^o)/\tau_w(fq^o)]}{(1-f)q^o dp},$$

where f is a fraction (e.g., 0.9). Since (A7) is nonlinear (i.e., W_T and W_q depend on T and q), it must be solved iteratively by recomputing W_T and W_q from the prior solution for T and q during the iterative process.

Acknowledgments. The authors wish to acknowledge the support of this work by the Department of Energy under Grant DE-FG-02-92ER61365. The continued support of Gerry Stokes, Ted Cress, and Dave Turner of the DOE Atmospheric Radiation Measurement Program is greatly appreciated.

REFERENCES

Businger, S., and Coauthors, 1996: The promise of GPS in atmospheric monitoring. *Bull. Amer. Meteor. Soc.,* **77,** 5–18.

Clough, S. A., F. X. Kneizys, L. S. Rothman, and W. O. Gallery, 1981: Atmospheric spectra transmittance and radiance: FASCODE1B. *SPIE Atmos. Transmission,* **277,** 152.

——, ——, and R. W. Davies, 1989: Line shape and the water vapor continuum. *Atmos. Res.,* **23,** 229.

Eyre, J. R., 1991: A fast radiative transfer model for satellite sounding systems. ECMWF Research Department Tech. Memo. 176, ECMWF, Reading, United Kingdom. [Available from ECMWF Library, Shinfield Park, Reading RG2 9AX, United Kingdom.]

Feltz, W., 1994: Meteorological applications of the atmospheric emitted radiance interferometer (AERI). M.S. thesis, Department of Atmospheric and Oceanic Sciences, University of Wisconsin—Madison, 87 pp. [Available from University of Wisconsin—Madison, Schwerdtfeger Library, 1225 W. Dayton, Madison, Wisconsin 53705].

——, W. L. Smith, R. O. Knuteson, and H. E. Revercomb, 1995: Meteorological applications of the Atmospheric Emitted Radiance Interferometer (AERI). *Proc. Optical Remote Sensing of the Atmosphere Conf.,* Salt Lake City, UT, Optical Society of America, 111–113.

——, ——, ——, ——, and B. Howell, 1996: AERI temperature and water vapor retrievals: Improvements using an integrated profile retrieval approach. *Proc. Fifth ARM Science Team Meeting,* San Antonio, TX, Department of Energy, 81–83.

——, ——, ——, ——, ——, and H. M. Woolf, 1998: Meteorological applications of temperature and water vapor retrievals from the ground-based Atmospheric Emitted Radiance Interferometer (AERI). *J. Appl. Meteor.,* **37,** 857–875.

Goldsmith, J. E. M., S. E. Bisson, R. A. Ferrare, K. D. Evans, D. N. Whiteman, and S. H. Melfi, 1994: Raman lidar profiling of atmospheric water vapor: Simultaneous measurements with two collocated systems. *Bull. Amer. Meteor. Soc.,* **75,** 975–982.

Han, Y., J. Snider, E. Westwater, S. Melfi, and R. Ferrare, 1994: Observations of water vapor by ground-based microwave radiometers and Raman lidar. *J. Geophys. Res.*, **99,** 18 695–18 702.

Melfi, S. H., and D. N. Whiteman, 1985: Observation of lower atmospheric moisture structure and its evolution using a Raman lidar. *Bull. Amer. Meteor. Soc.,* **66,** 1288–1292.

Pratt, R. W., 1985: Review of radiosonde humidity and temperature errors. *J. Atmos. Oceanic Technol.,* **2,** 404–407.

Revercomb, H., H. Buijs, H. B. Howell, D. D. LaPorte, W. L. Smith, and L. A. Sromovsky, 1988: Radiometric calibration of IR Fourier transform spectrometers: Solution to a problem with the high-resolution spectrometer sounder. *Appl. Opt.,* **27,** 3210–3218.

——, and Coauthors, 1993: Atmospheric Emitted Radiance Interferometer (AERI) for ARM. Preprints, *Fourth Symp. on Global Change Studies,* Anaheim, CA, Amer. Meteor. Soc., 46–49.

Rothman, L. S., and Coauthors, 1992: The HITRAN molecular database: Editions of 1991 and 1992. *J. Quant. Spectros. Radiat. Transfer,* **48,** 469.

Schmidlin, F. J., 1988: WMO international radiosonde comparison, phase II final report, 1985. Instruments and Observing Methods Report 29 WMO/TD 312. [Available from WMO Secretariat, 41 ave. Giuseppe Motta Case Postale 2300, CH-1211 Geneva 2, Switzerland.]

Smith, W. L., 1970: Iterative solution of the radiative transfer equation for the temperature and absorbing gas profile of an atmosphere. *Appl. Opt.,* **9,** 9.

——, and Coauthors, 1990: GAPEX: A ground-based atmospheric profiling experiment. *Bull. Amer. Meteor. Soc.,* **71,** 3.

——, R. O. Knuteson, H. E. Revercomb, F. A. Best, R. G. Dedecker, and H. B. Howell, 1993: GB-HIS: A measurement system for continuous profiling of boundary layer thermodynamic structure. *Proc. Eighth Symp. on Meteorological Observations and Instrumentation,* Anaheim, CA, Amer. Meteor. Soc., 180–183.

——, W. F. Feltz, R. O. Knuteson, and H. E. Revercomb, 1995: PBL sounding and cloud emittance observations with ARM-CART AERI observations. *Proc. Fourth ARM Science Team Meeting,* San Diego, CA, Department of Energy, 203–205.

Spänkuch, D., W. Döhler, J. Güldner, and A. Keens, 1995: Ground-based passive atmospheric remote sounding by FTIR emission spectroscopy—First results with EISAR. *Beitr. Phys. Atmos.,* **69,** 97–111.

Ware, R. H., and Coauthors, 1996: GPS sounding of the atmosphere from low earth orbit: Preliminary results. *Bull. Amer. Meteor. Soc.,* **77,** 19–40.